Commun. Comput. Phys.
doi: 10.4208/cicp.070215.200715a

Vol. **xx**, No. x, pp. 1-26
xxx 201x

Runge-Kutta Discontinuous Galerkin Method with a Simple and Compact Hermite WENO Limiter

Jun Zhu[1], Xinghui Zhong[2], Chi-Wang Shu[3] and Jianxian Qiu[4,*]

[1] *College of Science, Nanjing University of Aeronautics and Astronautics, Nanjing, Jiangsu 210016, P.R. China.*
[2] *Department of Mathematics, Michigan State University, East Lansing, MI 48824, USA.*
[3] *Division of Applied Mathematics, Brown University, Providence, RI 02912, USA.*
[4] *School of Mathematical Sciences and Fujian Provincial Key Laboratory of Mathematical Modeling and High-Performance Scientific Computation, Xiamen University, Xiamen, Fujian 361005, P.R. China.*

Received xxx; Accepted (in revised version) xxx

Abstract. In this paper, we propose a new type of weighted essentially non-oscillatory (WENO) limiter, which belongs to the class of Hermite WENO (HWENO) limiters, for the Runge-Kutta discontinuous Galerkin (RKDG) methods solving hyperbolic conservation laws. This new HWENO limiter is a modification of the simple WENO limiter proposed recently by Zhong and Shu [29]. Both limiters use information of the DG solutions only from the target cell and its immediate neighboring cells, thus maintaining the original compactness of the DG scheme. The goal of both limiters is to obtain high order accuracy and non-oscillatory properties simultaneously. The main novelty of the new HWENO limiter in this paper is to reconstruct the polynomial on the target cell in a least square fashion [8] while the simple WENO limiter [29] is to use the entire polynomial of the original DG solutions in the neighboring cells with an addition of a constant for conservation. The modification in this paper improves the robustness in the computation of problems with strong shocks or contact discontinuities, without changing the compact stencil of the DG scheme. Numerical results for both one and two dimensional equations including Euler equations of compressible gas dynamics are provided to illustrate the viability of this modified limiter.

AMS subject classifications: 65M60, 35L65

Key words: Runge-Kutta discontinuous Galerkin method, HWENO limiter, conservation law.

*Corresponding author. *Email addresses:* zhujun@nuaa.edu.cn (J. Zhu), zhongxh@math.msu.edu (X. Zhong), shu@dam.brown.edu (C.-W. Shu), jxqiu@xmu.edu.cn (J. Qiu)

1 Introduction

In this paper, we are interested in solving the hyperbolic conservation law

$$\begin{cases} u_t + f(u)_x = 0, \\ u(x,0) = u_0(x), \end{cases} \tag{1.1}$$

and its two-dimensional version

$$\begin{cases} u_t + f(u)_x + g(u)_y = 0, \\ u(x,y,0) = u_0(x,y), \end{cases} \tag{1.2}$$

using the Runge-Kutta discontinuous Galerkin (RKDG) methods [4–7], where u, $f(u)$ and $g(u)$ can be either scalars or vectors.

It is not an easy task to solve (1.1) and (1.2) since solutions may contain discontinuities even if the initial conditions are smooth. Discontinuous Galerkin (DG) methods can capture weak shocks and other discontinuities without further modification. However, for problems with strong discontinuous solutions, the numerical solution has significant oscillations near discontinuities, especially for high order methods. A common strategy to control these spurious oscillations is to apply a nonlinear limiter. One type of limiters is based on the slope methodology, such as the *minmod* type limiters [4–7], the moment based limiter [2] and an improved moment limiter [3]. These limiters do control the oscillations well, however they may degrade accuracy when mistakenly used in smooth regions of the solution. Another type of limiters is based on the weighted essentially non-oscillatory (WENO) methodology [11–13,17], which can achieve both high order accuracy and non-oscillatory properties. The WENO limiters introduced in [18–20,22,30] and the Hermite WENO limiters in [19,22] belong to this type. These limiters are designed based on the WENO finite volume methodology which require a wider stencil for higher order schemes. Therefore, it is difficult to implement them for multi-dimensional problems, especially on unstructured meshes. An alternative family of DG limiters which serves at the same time as a new PDE-based limiter, as well as a troubled cells indicator, was introduced by Dumbser et al. [10].

More recently, a particularly simple and compact WENO limiter, which utilizes fully the advantage of DG schemes in that a complete polynomial is available in each cell without the need of reconstruction, is designed for RKDG schemes in [29]. The two major advantages of this simple WENO limiter are the compactness of its stencil, which contains only immediate neighboring cells, and the simplicity in implementation, especially for unstructured meshes [31]. However, it was observed in [29] that the limiter might not be robust enough for problems containing very strong shocks or low pressure problem, especially for higher order polynomials, for example the blast wave problems [23,28] and the double rarefaction wave problem [16], making it necessary to apply additional positivity-preserving limiters [27] in such situation. In order to overcome this difficulty, without compromising the advantages of compact stencil and simplicity of linear weights, we present a modification of the limiter in the step of preprocessing the

polynomials in the immediate neighboring cells before applying the WENO reconstruction procedure. This preprocessing is necessary to maintain strict conservation, and is designed in [29] to be a simple addition of a constant to make the cell average of the preprocessed neighboring cell polynomial in the target cell matching the original cell average. In this paper, a more involved least square process [8] is used in this step. The objective is to achieve strict conservation while maintaining more information of the original neighboring cell polynomial before applying the WENO procedure. Numerical experiments indicate that this modification does improve the robustness of the limiter.

This paper is organized as follows: In Section 2, we provide a brief review of RKDG for one dimensional and two dimensional cases. In Section 3, we provide the details of the new HWENO limiter for one dimensional scalar and system cases. In Section 4, we provide the details of the HWENO limiter for two dimensional scalar and system cases. We demonstrate the performance of our HWENO limiter with one and two dimensional numerical examples including Euler equations of compressible gas dynamics in Section 5. Concluding remarks are given in Section 6.

2 Review of RKDG methods

In this subsection, we give a brief review of the RKDG methods for solving one and two dimensional conservation laws.

One dimensional case. Given a partition of the computational domain consisting of cells $I_j=[x_{j-\frac{1}{2}},x_{j+\frac{1}{2}}]$, $j=1,\cdots,N$, denote the cell center by $x_j=\frac{1}{2}(x_{j-\frac{1}{2}}+x_{j+\frac{1}{2}})$, and the cell size by $\Delta x_j=x_{j+\frac{1}{2}}-x_{j-\frac{1}{2}}$. The DG method has its solution as well as the test function space given by $V_h^k=\{v(x):v(x)|_{I_j}\in\mathbb{P}^k(I_j)\}$, where $\mathbb{P}^k(I_j)$ denotes the set of polynomials of degree at most k defined on I_j. The semi-discrete DG method for solving (1.1) is defined as follows: find the unique function $u_h(\cdot,t)\in V_h^k$ such that for $j=1,\cdots,N$,

$$\int_{I_j}(u_h)_t v\,dx-\int_{I_j}f(u_h)v_x\,dx+\hat{f}_{j+\frac{1}{2}}v(x_{j+\frac{1}{2}}^-)-\hat{f}_{j-\frac{1}{2}}v(x_{j-\frac{1}{2}}^+)=0 \tag{2.1}$$

holds for all test functions $v\in V_h^k$, where $u_{j+\frac{1}{2}}^{\pm}=u_h(x_{j+\frac{1}{2}}^{\pm},t)$ are the left and right limits of the discontinuous solution u_h at the interface $x_{j+\frac{1}{2}}$ and $\hat{f}_{j+\frac{1}{2}}=\hat{f}(u_{j+\frac{1}{2}}^-,u_{j+\frac{1}{2}}^+)$ is a monotone flux for the scalar case and an exact or approximate Riemann solver for the system case.

Two dimensional case. Given a partition of the computational domain consisting of rectangular mesh consisting of cells $I_{ij}=[x_{i-\frac{1}{2}},x_{i+\frac{1}{2}}]\times[y_{j-\frac{1}{2}},y_{j+\frac{1}{2}}]$, for $i=1,\cdots,N_x$ and $j=1,\cdots,N_y$ with the cell sizes $x_{i+\frac{1}{2}}-x_{i-\frac{1}{2}}=\Delta x_i$, $y_{j+\frac{1}{2}}-y_{j-\frac{1}{2}}=\Delta y_j$ and cell centers $(x_i,y_j)=(\frac{1}{2}(x_{i+\frac{1}{2}}+x_{i-\frac{1}{2}}),\frac{1}{2}(y_{j+\frac{1}{2}}+y_{j-\frac{1}{2}}))$. We now give the new test function space $W_h^k=\{p:p|_{I_{ij}}\in\mathbb{P}^k(I_{ij})\}$ as the polynomial spaces of degree of at most k on the cell I_{ij}. The semi-discrete DG method for solving (1.2) is defined as follows: find the unique function $u\in W_h^k$ such

that, for all $1\le i\le N_x$ and $1\le j\le N_y$,

$$\begin{aligned}&\int_{I_{i,j}}(u_h)_t v dxdy\\ =&\int_{I_{i,j}} f(u_h)v_x dxdy-\int_{I_j}\hat{f}_{i+\frac{1}{2}}(y)v(x^-_{i+\frac{1}{2}},y)dy+\int_{I_j}\hat{f}_{i-\frac{1}{2}}(y)v(x^+_{i-\frac{1}{2}},y)dy\\ &+\int_{I_{i,j}} g(u_h)v_y dxdy-\int_{I_i}\hat{g}_{j+\frac{1}{2}}(x)v(x,y^-_{j+\frac{1}{2}})dx+\int_{I_i}\hat{g}_{i-\frac{1}{2}}(x)v(x,y^+_{j-\frac{1}{2}})dx,\end{aligned}\tag{2.2}$$

hold for all the test function $v\in W_h^k$, where the "hat" terms are again numerical fluxes.

The semi-discrete schemes (2.1) and (2.2) can be written as

$$u_t=L(u),$$

where $L(u)$ is the spatial discretization operator. They can be discretized in time by a non-linearly stable Runge-Kutta time discretization [25], e.g. the third-order version:

$$\begin{aligned}u^{(1)}&=u^n+\Delta tL(u^n),\\ u^{(2)}&=\frac{3}{4}u^n+\frac{1}{4}u^{(1)}+\frac{1}{4}\Delta tL(u^{(1)}),\\ u^{n+1}&=\frac{1}{3}u^n+\frac{2}{3}u^{(2)}+\frac{2}{3}\Delta tL(u^{(2)}).\end{aligned}\tag{2.3}$$

As in [29], to apply a nonlinear limiter for the RKDG methods, for simplicity, we take the forward Euler time discretization of the semi-discrete scheme (2.1) as an example. Starting from a solution $u_h^n\in V_h^k$ at time level n (u_h^0 is taken as the L^2 projection of the analytical initial condition into V_h^k). We would like to "limit" it to obtain a new function $u^{n,new}$ before advancing it to next time level. That is: find $u_h^{n+1}\in V_h^k$, such that, for $j=1,\cdots,N$,

$$\int_{I_j}\frac{u_h^{n+1}-u_h^{n,new}}{\Delta t}v dx-\int_{I_j} f(u_h^{n,new})v_x\,dx+\hat{f}^{n,new}_{j+\frac{1}{2}}v(x^-_{j+\frac{1}{2}})-\hat{f}^{n,new}_{j-\frac{1}{2}}v(x^+_{j-\frac{1}{2}})=0\tag{2.4}$$

holds for all test functions $v\in V_h^k$. The limiting procedure to go from u_h^n to $u_h^{n,new}$ will be discussed in the following sections.

3 New HWENO limiter in one dimension

In this section, we describe the details of the modified HWENO reconstruction procedure as a limiter for the RKDG method in the one dimensional scalar and system cases.

3.1 The troubled cell indicator in one dimension

An important component of the simple WENO limiter in [29] is the identification of troubled cells, which are cells that may contain discontinuities and in which the WENO limiter is applied. We will use the KXRCF shock detection technique developed in [15] to detect troubled cells. We divide the boundary of the target cell I_j into two parts: ∂I_j^- and ∂I_j^+, where the flow is into ($v\cdot n<0$, n is the normal vector to ∂I_j and v is the velocity) and out of ($v\cdot n>0$) I_j, respectively. Here, we define v, taking its value from inside the cell I_j as $f'(u)$ and take u as the indicator variable for the scalar case. The target cell I_j is identified as a troubled cell when

$$\frac{|\int_{\partial I_j^-}(u_h(x,t)|_{I_j}-u_h(x,t)|_{I_l})ds|}{\Delta x_j^{\frac{k+1}{2}}|\partial I_j^-|\cdot||u_h(x,t)|_{I_j}||}>C_k, \tag{3.1}$$

where C_k is a constant, usually, we take $C_k=1$ as in [15]. Here I_l, for $l=j-1$ or $j+1$, denotes the neighboring cell sharing the end point ∂I_j^- with I_j. u_h is the numerical solution corresponding to the indicator variable(s) and $||u_h(x,t)|_{I_j}||$ is the standard L^2 norm in the cell I_j.

3.2 HWENO limiting procedure in one dimension: scalar case

In this subsection, we present the details of the HWENO limiting procedure for the scalar case. The idea of this new HWENO limiter is to reconstruct a new polynomial on the troubled cell I_j which is a convex combination of three polynomials: the DG solution polynomial on this cell and the "modified" DG solution polynomials on its two immediate neighboring cells. The modification procedure is in a least square fashion [8]. The construction of the nonlinear weights in the convex combination coefficients follows the classical WENO procedure.

Assume I_j is a troubled cell.

Step 1.1. Denote the DG solution polynomials of u_h on I_{j-1},I_{j+1},I_j as polynomials $p_0(x)$, $p_1(x)$ and $p_2(x)$, respectively. Now we want to find the modified version of $p_0(x)$, denoted as $\tilde{p}_0(x)$ on the cell I_{j-1} in a least square fashion [8]. The modification procedure is defined as follows: $\tilde{p}_0(x)$ is the solution of the minimization problem

$$\min_{\forall\phi(x)\in\mathbb{P}^k(I_{j-1})}\left\{\int_{I_{j-1}}(\phi(x)-p_0(x))^2dx\right\}, \tag{3.2}$$

subject to $\bar{\bar{\phi}}=\bar{\bar{p}}_2$, where

$$\bar{\bar{\phi}}=\frac{1}{\Delta x_j}\int_{I_j}\phi(x)dx,\quad \bar{\bar{p}}_2=\frac{1}{\Delta x_j}\int_{I_j}p_2(x)dx.$$

Here and below $\bar{\bar{\star}}$ denotes the cell average of the function $\star$ on the target cell.

Similarly, $\tilde{p}_1(x)$ is the solution of the minimization problem

$$\min_{\forall \phi(x)\in \mathbb{P}^k(I_{j+1})} \left\{ \int_{I_{j+1}} (\phi(x)-p_1(x))^2 dx \right\} \tag{3.3}$$

subject to $\bar{\tilde{\phi}} = \bar{\tilde{p}}_2$.

For notational consistency we denote $\tilde{p}_2(x) = p_2(x)$.

The final nonlinear HWENO reconstruction polynomial $p_2^{new}(x)$ is now defined by a convex combination of these modified polynomials:

$$p_2^{new}(x) = \omega_0 \tilde{p}_0(x) + \omega_1 \tilde{p}_1(x) + \omega_2 \tilde{p}_2(x). \tag{3.4}$$

According to the modification procedure, it is easy to prove that p_2^{new} has the same cell average and order of accuracy as p_2 if the weights satisfy $\omega_0+\omega_1+\omega_2 = 1$. The convex combination coefficients $\omega_l, l = 0,1,2$ follow the classical WENO procedure [1, 12, 13]. We discuss it in the following steps.

Step 1.2. We choose the linear weights denoted by $\gamma_0, \gamma_1, \gamma_2$. As in [29], we have used complete information of the three polynomials $p_0(x), p_1(x), p_2(x)$ in the three cells I_{j-1}, I_{j+1}, I_j, hence we do not have extra requirements on the linear weights in order to maintain the original high order accuracy. The linear weights can be chosen to be any set of positive numbers adding up to one. The choice of these linear weights is then solely based on the consideration of a balance between accuracy and ability to achieve essentially nonoscillatory shock transitions. In all of our numerical tests, following the practice in [9, 29], we take $\gamma_2 = 0.998$ and $\gamma_0 = \gamma_1 = 0.001$.

Step 1.3. We compute the smoothness indicators, denoted by β_ℓ, $\ell = 0,1,2$, which measure how smooth the functions $\tilde{p}_\ell(x)$, $\ell = 0,1,2$, are on the target cell I_j. The smaller these smoothness indicators are, the smoother the functions are on the target cell. We use the similar recipe for the smoothness indicators as in [13]:

$$\beta_\ell = \sum_{l=1}^{k} \Delta x_j^{2l-1} \int_{I_j} \left(\frac{1}{l!} \frac{d^l}{dx^l} \tilde{p}_\ell(x) \right)^2 dx, \quad \ell = 0,1,2. \tag{3.5}$$

Step 1.4. We compute the non-linear weights based on the smoothness indicators:

$$\omega_i = \frac{\bar{\omega}_i}{\sum_{\ell=0}^{2} \bar{\omega}_\ell}, \qquad \bar{\omega}_\ell = \frac{\gamma_\ell}{(\varepsilon+\beta_\ell)^2}. \tag{3.6}$$

Here ε is a small positive number to avoid the denominator to become zero. We take $\varepsilon = 10^{-6}$ in our computation.

Step 1.5. The final nonlinear HWENO reconstruction polynomial is given by (3.4), i.e. $u_h^{new}|_{I_j} = p_2^{new}(x) = \omega_0 \tilde{p}_0(x) + \omega_1 \tilde{p}_1(x) + \omega_2 \tilde{p}_2(x)$.

It is easy to verify that $p_2^{new}(x)$ has the same cell average and order of accuracy as the original one $p_2(x)$, on the condition that $\sum_{\ell=0}^{2} \omega_\ell = 1$.

3.3 HWENO limiting procedure in one dimension: system case

In this subsection, we present the details of the HWENO limiting procedure for one dimensional systems.

Consider Eq. (1.1) where u and $f(u)$ are vectors with m components. In order to achieve better non-oscillatory qualities, the HWENO reconstruction limiter is used with a local characteristic field decomposition. In this paper, we consider the following Euler system with $m=3$.

$$\frac{\partial}{\partial t}\begin{pmatrix}\rho\\ \rho\mu\\ E\end{pmatrix}+\frac{\partial}{\partial x}\begin{pmatrix}\rho\mu\\ \rho\mu^2+p\\ \mu(E+p)\end{pmatrix}=0, \tag{3.7}$$

where ρ is the density, μ is the x-direction velocity, E is the total energy, p is the pressure and $\gamma=1.4$ in our test cases. We denote the Jacobian matrix as $f'(u)$, where $u=(\rho,\rho\mu,E)^T$. We then give the left and right eigenvector matrices of such Jacobian matrix as:

$$L_j(u)=\begin{pmatrix}\frac{B_2+\mu/c}{2} & -\frac{B_1\mu+1/c}{2} & \frac{B_1}{2}\\ 1-B_2 & B_1\mu & -B_1\\ \frac{B_2-\mu/c}{2} & -\frac{B_1\mu-1/c}{2} & \frac{B_1}{2}\end{pmatrix}, \tag{3.8}$$

and

$$R_j(u)=\begin{pmatrix}1 & 1 & 1\\ \mu-c & \mu & \mu+c\\ H-c\mu & \mu^2/2 & H+c\mu\end{pmatrix}, \tag{3.9}$$

where $c=\sqrt{\gamma p/\rho}$, $B_1=(\gamma-1)/c^2$, $B_2=B_1\mu^2/2$ and $H=(E+p)/\rho$.

Assume the troubled cell I_j is detected by the KXRCF technique [15] by using (3.1), where $v=\mu$ is the velocity and again v takes its value from inside the cell I_j. We take both the density ρ and the total energy E as the indicator variables. Denote p_0, p_1, p_2 to be the DG polynomial vectors, corresponding to I_j's two immediate neighbors and itself. Then we perform the characteristic-wise HWENO limiting procedure as follows:

Step 2.1. Compute $L_j=L_j(\bar{u}_j)$ and $R_j=R_j(\bar{u}_j)$ as defined in (3.8) and (3.9), where $\bar{u}_j$ is the cell average of u on the cell I_j.

Step 2.2. Project the polynomial vectors p_0, p_1, p_2 into the characteristic fields $\tilde{p}_\ell = L_j p_\ell$, $\ell=0,1,2$, each of them being a 3-component vector and each component of the vector is a k-th degree polynomial.

Step 2.3. Perform Step 1.1 to Step 1.5 of the HWENO limiting procedure that has been specified for the scalar case, to obtain a new 3-component vector on the troubled cell I_j as $\tilde{p}_2^{new}$.

Step 2.4. Project $\tilde{p}_2^{new}$ back into the physical space to get the reconstruction polynomial, i.e. $u_h^{new}|_{I_j}=R_j\tilde{p}_2^{new}$.

4 New HWENO limiter in two dimension

4.1 The troubled cell indicator in two dimension

We use the KXRCF shock detection technique developed in [15] to detect troubled cells in two dimensions. We divide the boundary of the target cell I_{ij} into two parts: ∂I_{ij}^- and ∂I_{ij}^+, where the flow is into ($v\cdot n<0$, n is the normal vector to ∂I_{ij}) and out of ($v\cdot n>0$) I_{ij}, respectively. Here we define v, taking its value from inside the cell I_{ij}, as the vector $(f'(u),g'(u))$ and take u as the indicator variable for the scalar case. For the Euler system (4.4), v, again taking its value from inside the cell I_{ij}, is (μ,ν) where μ is the x-direction velocity and ν is the y-direction velocity, and we take both the density ρ and the total energy E as the indicator variables. The target cell I_{ij} is identified as a troubled cell when

$$\frac{|\int_{\partial I_{ij}^-}(u_h(x,y,t)|_{I_{ij}}-u_h(x,y,t)|_{I_l})ds|}{h_{ij}^{\frac{k+1}{2}}|\partial I_{ij}^-|\cdot||u_h(x,y,t)|_{I_{ij}}||}>C_k, \tag{4.1}$$

where C_k is a constant, usually, we take $C_k=1$ as in [15]. Here we choose h_{ij} as the radius of the circumscribed circle in I_{ij}, and I_l,$l=(i,j-1)$; $(i-1,j)$; $(i+1,j)$; $(i,j+1)$, denote the neighboring cells sharing the edge(s) in ∂I_{ij}^-. u_h is the numerical solution corresponding to the indicator variable(s) and $||u_h(x,y,t)|_{I_{ij}}||$ is the standard L^2 norm in the cell I_{ij}.

4.2 HWENO limiting procedure in two dimensions: scalar case

In this subsection, we give details of the HWENO limiter for the two dimensional scalar case.

The idea is similar to the one dimensional case, i.e. to reconstruct a new polynomial on the troubled cell I_{ij} which is a convex combination of the following polynomials: DG solution polynomial on this cell and the "modified" DG solution polynomials on its immediate neighboring cells. The nonlinear weights in the convex combination coefficients follow the classical WENO procedure. To achieve better non-oscillatory property, the modification procedure now is in a least square fashion [8] with necessary adjustment.

Assume I_{ij} is a troubled cell.

Step 3.1. We select the HWENO reconstruction stencil as $S=\{I_{i-1,j}, I_{i,j-1}, I_{i+1,j}, I_{i,j+1}, I_{ij}\}$, for simplicity, we renumber these cells as I_ℓ, $\ell=0,\cdots,4$, and denote the DG solutions on these five cells to be $p_\ell(x,y)$, respectively. Now we want to find the modified version of $p_\ell(x,y)$, denoted as $\tilde{p}_\ell(x,y)$, in a least square fashion [8] with necessary adjustment. The modification procedure not only use the complete information of the polynomial $p_\ell(x,y)$, but also use the cell averages of the polynomials from its other neighbors.

For $p_0(x,y)$, the modification procedure is defined as follows: $\tilde{p}_0(x,y)$ is the solution

of the minimization problem

$$\min_{\forall \phi(x,y)\in \mathbb{P}^k(I_0)} \left\{ \left(\int_{I_0} (\phi(x,y)-p_0(x,y))^2 dxdy \right) + \sum_{\ell\in\mathbb{L}_0} \left(\int_{I_\ell} (\phi(x,y)-p_\ell(x,y))dxdy \right)^2 \right\},$$

subject to $\bar{\bar{\phi}} = \bar{\bar{p}}_4$ and

$$\mathbb{L}_0 = \{1,2,3\} \cap \{\ell : |\bar{p}_\ell - \bar{p}_4| < \max(|\bar{p}_1-\bar{p}_4|, |\bar{p}_2-\bar{p}_4|, |\bar{p}_3-\bar{p}_4|)\},$$

where $\bar{p}_\ell = \frac{1}{|I_\ell|}\int_{I_\ell} p_\ell(x,y)dxdy$ is the cell average of the polynomial $p_\ell(x,y)$ on the cell I_ℓ and $|I_\ell|$ is the area of I_ℓ. Here and below $\bar{\star}$ denotes the cell average of the function $\star$ on its own associated cell.

For this modification, we try to find the polynomial $\tilde{p}_0$, which has the same cell average as the polynomial on the troubled cell p_4, to optimize the distance to $p_0(x,y)$ and to the cell averages of those "useful" polynomials on the other neighboring cells. By comparing the distance between the cell averages of the polynomials on the other neighboring cells and the cell average of p_4 on the target cell, if one is not the farthest, then this polynomial is considered "useful".

Remark 4.1. The one dimensional algorithm is consistent with the two dimensional one, because in one dimension we only have two immediate neighbors and hence $\mathbb{L}=\emptyset$ is the empty set. In the extreme case (for example, if $|\bar{p}_1-\bar{p}_4| = |\bar{p}_2-\bar{p}_4| = |\bar{p}_3-\bar{p}_4|$), this two dimensional algorithm could degenerate to the one dimensional case and $\mathbb{L}_0$ could also be $\emptyset$.

Similarly, $\tilde{p}_1(x,y)$ is the solution of the minimization problem

$$\min_{\forall \phi(x,y)\in \mathbb{P}^k(I_1)} \left\{ \left(\int_{I_1} (\phi(x,y)-p_1(x,y))^2 dxdy \right) + \sum_{\ell\in\mathbb{L}_1} \left(\int_{I_\ell} (\phi(x,y)-p_\ell(x,y))dxdy \right)^2 \right\},$$

subject to $\bar{\bar{\phi}} = \bar{\bar{p}}_4$, where

$$\mathbb{L}_1 = \{0,2,3\} \cap \{\ell : |\bar{p}_\ell - \bar{p}_4| < \max(|\bar{p}_0-\bar{p}_4|, |\bar{p}_2-\bar{p}_4|, |\bar{p}_3-\bar{p}_4|)\}.$$

$\tilde{p}_2(x,y)$ is the solution of the minimization problem

$$\min_{\forall \phi(x,y)\in \mathbb{P}^k(I_2)} \left\{ \left(\int_{I_2} (\phi(x,y)-p_2(x,y))^2 dxdy \right) + \sum_{\ell\in\mathbb{L}_2} \left(\int_{I_\ell} (\phi(x,y)-p_\ell(x,y))dxdy \right)^2 \right\},$$

subject to $\bar{\bar{\phi}} = \bar{\bar{p}}_4$, where

$$\mathbb{L}_2 = \{0,1,3\} \cap \{\ell : |\bar{p}_\ell - \bar{p}_4| < \max(|\bar{p}_0-\bar{p}_4|, |\bar{p}_1-\bar{p}_4|, |\bar{p}_3-\bar{p}_4|)\}.$$

$\tilde{p}_3(x,y)$ is the solution of the minimization problem

$$\min_{\forall \phi(x,y)\in \mathbb{P}^k(I_3)} \left\{ \left(\int_{I_3} (\phi(x,y)-p_3(x,y))^2 dxdy \right) + \sum_{\ell\in \mathbb{L}_3} \left(\int_{I_\ell} (\phi(x,y)-p_\ell(x,y)) dxdy \right)^2 \right\},$$

subject to $\bar{\tilde{\phi}} = \bar{\tilde{p}}_4$, where

$$\mathbb{L}_3 = \{0,1,2\} \cap \{\ell : |\bar{p}_\ell - \bar{p}_4| < \max(|\bar{p}_0-\bar{p}_4|, |\bar{p}_1-\bar{p}_4|, |\bar{p}_2-\bar{p}_4|)\}.$$

We also define $\tilde{p}_4(x,y) = p_4(x,y)$.

Step 3.2. We choose the linear weights denoted by $\gamma_0,\gamma_1,\gamma_2,\gamma_3,\gamma_4$. Similar as in the one dimensional case, we put a larger linear weight on the troubled cell and the neighboring cells get smaller linear weights. In all of our numerical tests, following the practice in [9,29], we take $\gamma_4 = 0.996$ and $\gamma_0 = \gamma_1 = \gamma_2 = \gamma_3 = 0.001$.

Step 3.3. We compute the smoothness indicators, denoted by β_ℓ, $\ell = 0,\cdots,4$, which measure how smooth the functions $\tilde{p}_\ell(x,y)$, $\ell = 0,\cdots,4$, are on the target cell I_{ij}. We use the similar recipe for the smoothness indicators as in [1,13,24]:

$$\beta_\ell = \sum_{|\alpha|=1}^{k} |I_{ij}|^{|\alpha|-1} \int_{I_{ij}} \left(\frac{1}{|\alpha|!} \frac{\partial^{|\alpha|}}{\partial x^{\alpha_1} \partial y^{\alpha_2}} \tilde{p}_\ell(x,y) \right)^2 dxdy, \quad \ell = 0,\cdots,4, \tag{4.2}$$

where $\alpha = (\alpha_1,\alpha_2)$ and $|\alpha| = \alpha_1 + \alpha_2$.

Step 3.4. We compute the nonlinear weights based on the smoothness indicators.

Step 3.5. The final nonlinear HWENO reconstruction polynomial $p_4^{new}(x,y)$ is defined by a convex combination of the (modified) polynomials in the stencil:

$$u_h^{new}|_{I_{ij}} = p_4^{new}(x,y) = \sum_{\ell=0}^{4} \omega_\ell \tilde{p}_\ell(x,y). \tag{4.3}$$

It is easy to verify that $p_4^{new}(x,y)$ has the same cell average and order of accuracy as the original one $p_4(x,y)$ on the condition that $\sum_{\ell=0}^{4} \omega_\ell = 1$.

4.3 HWENO limiting procedure in two dimensions: system case

In this subsection, we present the details of the HWENO limiting procedure for two dimensional systems.

Consider Eq. (1.2) where u, $f(u)$ and $g(u)$ are vectors with m components. In order to achieve better non-oscillatory qualities, the HWENO reconstruction limiter is used with

a local characteristic field decomposition. In this paper, we only consider the following Euler system with $m=4$.

$$\frac{\partial}{\partial t}\begin{pmatrix}\rho\\ \rho\mu\\ \rho\nu\\ E\end{pmatrix}+\frac{\partial}{\partial x}\begin{pmatrix}\rho\mu\\ \rho\mu^2+p\\ \rho\mu\nu\\ \mu(E+p)\end{pmatrix}+\frac{\partial}{\partial y}\begin{pmatrix}\rho\nu\\ \rho\mu\nu\\ \rho\nu^2+p\\ \nu(E+p)\end{pmatrix}=0, \tag{4.4}$$

where ρ is the density, μ is the x-direction velocity, ν is the y-direction velocity, E is the total energy, p is the pressure and $\gamma=1.4$ in our test cases. We then give the left and right eigenvector matrices of Jacobian matrices $f'(u)$ and $g'(u)$ as:

$$L^x_{ij}(u)=\begin{pmatrix}\frac{B_2+\mu/c}{2} & -\frac{B_1\mu+1/c}{2} & -\frac{B_1\nu}{2} & \frac{B_1}{2}\\ \nu & 0 & -1 & 0\\ 1-B_2 & B_1\mu & B_1\nu & -B_1\\ \frac{B_2-\mu/c}{2} & -\frac{B_1\mu-1/c}{2} & -\frac{B_1\nu}{2} & \frac{B_1}{2}\end{pmatrix}, \tag{4.5}$$

$$R^x_{ij}(u)=\begin{pmatrix}1 & 0 & 1 & 1\\ \mu-c & 0 & \mu & \mu+c\\ \nu & -1 & \nu & \nu\\ H-c\mu & -\nu & \frac{\mu^2+\nu^2}{2} & H+c\mu\end{pmatrix}, \tag{4.6}$$

$$L^y_{ij}(u)=\begin{pmatrix}\frac{B_2+\nu/c}{2} & -\frac{B_1\mu}{2} & -\frac{B_1\nu+1/c}{2} & \frac{B_1}{2}\\ -\mu & 1 & 0 & 0\\ 1-B_2 & B_1\mu & B_1\nu & -B_1\\ \frac{B_2-\nu/c}{2} & -\frac{B_1\mu}{2} & -\frac{B_1\nu-1/c}{2} & \frac{B_1}{2}\end{pmatrix}, \tag{4.7}$$

$$R^y_{ij}(u)=\begin{pmatrix}1 & 0 & 1 & 1\\ \mu & 1 & \mu & \mu\\ \nu-c & 0 & \nu & \nu+c\\ H-c\nu & \mu & \frac{\mu^2+\nu^2}{2} & H+c\nu\end{pmatrix}, \tag{4.8}$$

where $c=\sqrt{\gamma p/\rho}$, $B_1=(\gamma-1)/c^2$, $B_2=B_1(\mu^2+\nu^2)/2$ and $H=(E+p)/\rho$. The troubled cell I_{ij} is detected by the KXRCF technique [15] using (4.1). Denote p_ℓ, $\ell=0,\cdots,4$, to be the

DG polynomial vectors, corresponding to I_{ij}'s four immediate neighbors and itself. The HWENO limiting procedure is then performed as follows:

Step 4.1. We reconstruct the new polynomial vectors $p_4^{x,new}$ and $p_4^{y,new}$ by using the characteristic-wise HWENO limiting procedure:

– Step 4.1.1. Compute $L_{ij}^x = L_{ij}^x(\bar{u}_{ij})$, $L_{ij}^y = L_{ij}^y(\bar{u}_{ij})$, $R_{ij}^x = R_{ij}^x(\bar{u}_{ij})$ and $R_{ij}^y = R_{ij}^x(\bar{u}_{ij})$ as defined in (4.5)-(4.8), where again $\bar{u}_{ij}$ is the cell average of u on the cell I_{ij}.

– Step 4.1.2. Project the polynomial vectors p_ℓ, $\ell=0,\cdots,4$, into the characteristic fields $\tilde{p}_\ell^x = L_{ij}^x p_\ell$ and $\tilde{\tilde{p}}_\ell^y = L_{ij}^y p_\ell$, $\ell=0,\cdots,4$, each of them being a 4-component vector and each component of the vector is a k-th degree polynomial.

– Step 4.1.3. Perform Step 3.1 to Step 3.5 of the HWENO limiting procedure that has been specified for the scalar case, to obtain the new 4-component vectors on the troubled cell I_{ij} such as $\tilde{\tilde{p}}_4^{x,new}$ and $\tilde{\tilde{p}}_4^{y,new}$.

– Step 4.1.4. Project $\tilde{\tilde{p}}_4^{x,new}$ and $\tilde{\tilde{p}}_4^{y,new}$ into the physical space $p_4^{x,new} = R_{ij}^x \tilde{\tilde{p}}_4^{x,new}$ and $p_4^{y,new} = R_{ij}^y \tilde{\tilde{p}}_4^{y,new}$, respectively.

Step 4.2. The final new 4-component vector on the troubled cell I_{ij} is defined as $u_h^{new}|_{I_{ij}} = \frac{p_4^{x,new}+p_4^{y,new}}{2}$.

5 Numerical results

In this section, we provide numerical results to demonstrate the performance of the HWENO reconstruction limiters for the RKDG methods described in previous sections. We would like to remark that, for some cases with fourth order RKDG methods, the usage of the WENO limiters in [29] might not work well or might even break down, while the new HWENO limiters in this paper could obtain good resolutions. The simple Lax-Friedrichs flux is used in all of our numerical tests. We first test the accuracy of the schemes in one and two dimensional problems. We adjust the constant C_k in (3.1) or (4.1) to be a small number 0.001 from Example 5.1 to Example 5.4, for the purpose of artificially generating a larger percentage of troubled cells in order to test accuracy when the HWENO reconstruction procedure is enacted in more cells. In such test cases, we assume the coarse mesh as Γ_h, which has cell size h, and then divide each cell into two (in 1D) or four (in 2D) equal smaller cells and denote the associated fine mesh as $\Gamma_{\frac{h}{2}}$, which has smaller mesh size $\frac{h}{2}$. The error in the target cell I_i is set as e_i^h. The L^1 and L^∞ convergence errors in the computational field are defined as: $||e^h||_{L^1} = \frac{1}{N}\sum_{i=1}^N |e_i^h|$ and $||e^h||_{L^\infty} = \max_{1\le i\le N}|e_i^h|$, where N is the number of cells in the computational domain. The numerical order of accuracy are given by:

$$O_{L^1} = \log_2\left(\frac{||e^h||_{L^1}}{||e^{\frac{h}{2}}||_{L^1}}\right), \quad O_{L^\infty} = \log_2\left(\frac{||e^h||_{L^\infty}}{||e^{\frac{h}{2}}||_{L^\infty}}\right).$$

Table 1: $\mu_t+\left(\frac{\mu^2}{2}\right)_x=0$. $\mu(x,0)=0.5+\sin(\pi x)$. Periodic boundary condition. $t=0.5/\pi$. L^1 and L^∞ errors. RKDG with the HWENO limiter compared to RKDG without limiter.

		DG with HWENO limiter				DG without limiter			
	cells	L^1 error	order	L^∞ error	order	L^1 error	order	L^∞ error	order
P^1	10	2.00E-2		1.32E-1		1.38E-2		1.04E-1	
	20	5.62E-3	1.83	5.24E-2	1.33	3.52E-3	1.97	3.26E-2	1.67
	40	1.21E-3	2.21	1.26E-2	2.05	8.59E-4	2.03	9.11E-3	1.84
	80	2.23E-4	2.44	2.54E-3	2.31	2.11E-4	2.02	2.53E-3	1.85
	160	5.27E-5	2.08	6.74E-4	1.91	5.26E-5	2.00	6.72E-4	1.91
	320	1.31E-5	2.01	1.69E-4	1.99	1.31E-5	2.01	1.68E-4	1.99
P^2	10	1.74E-3		2.83E-2		1.72E-3		2.81E-2	
	20	2.06E-4	3.07	4.30E-3	2.72	2.02E-4	3.09	4.28E-3	2.72
	40	2.73E-5	2.91	6.94E-4	2.63	2.67E-5	2.93	6.78E-4	2.66
	80	3.43E-6	2.99	1.25E-4	2.46	3.32E-6	3.01	1.23E-4	2.45
	160	4.31E-7	2.99	1.60E-5	2.98	4.15E-7	2.99	1.53E-5	3.01
	320	5.44E-8	2.98	2.35E-6	2.76	5.27E-8	2.98	2.27E-6	2.76
P^3	10	1.80E-4		2.44E-3		1.76E-4		2.35E-3	
	20	1.69E-5	3.41	4.51E-4	2.43	1.66E-5	3.41	4.17E-4	2.50
	40	9.61E-7	4.14	3.83E-5	3.56	8.93E-7	4.22	3.67E-5	3.50
	80	6.52E-8	3.88	2.85E-6	3.75	5.40E-8	4.04	2.21E-6	4.05
	160	4.10E-9	3.99	2.14E-7	3.73	3.34E-9	4.01	1.43E-7	3.95
	320	2.08E-10	4.30	9.14E-9	4.55	2.08E-10	4.00	9.14E-9	3.97

The CFL number is set to be 0.3 for the second order (P^1), 0.18 for the third order (P^2) and 0.1 for the fourth order (P^3) RKDG methods both in one and two dimensions.

Example 5.1. We solve the following scalar Burgers equation:

$$\mu_t+\left(\frac{\mu^2}{2}\right)_x=0, \quad x\in[0,2], \tag{5.1}$$

with the initial condition $\mu(x,0)=0.5+\sin(\pi x)$ and periodic boundary conditions. We compute the solution up to $t=0.5/\pi$, when the solution is still smooth. The errors and numerical orders of accuracy for the RKDG method with the HWENO limiter comparing with the original RKDG method without a limiter are shown in Table 1. We can see that the HWENO limiter keeps the designed order of accuracy, even when a large percentage of good cells are artificially identified as troubled cells.

Example 5.2. We solve the 1D Euler equations (3.7). The initial conditions are: $\rho(x,0)=1+0.2\sin(\pi x)$, $\mu(x,0)=1.0$ and $p(x,0)=1$. The computing domain is $x\in[0,2]$. Periodic boundary conditions are applied in this test. The exact solution is $\rho(x,t)=1+0.2\sin(\pi(x-$

Table 2: 1D-Euler equations: initial data $\rho(x,0)=1+0.2\sin(\pi x)$, $\mu(x,0)=1.0$ and $p(x,0)=1$. Periodic boundary condition. $t=2.0$. L^1 and L^∞ errors. RKDG with the HWENO limiter compared to RKDG without limiter.

		DG with HWENO limiter				DG without limiter			
	cells	L^1 error	order	L^∞ error	order	L^1 error	order	L^∞ error	order
P^1	10	1.55E-2		3.53E-2		3.62E-3		8.29E-3	
	20	2.73E-3	2.50	9.49E-3	1.89	7.60E-4	2.25	2.68E-3	1.63
	40	3.28E-4	3.06	1.77E-3	2.41	1.73E-4	2.14	7.50E-4	1.84
	80	4.49E-5	2.87	2.57E-4	2.78	4.13E-5	2.07	1.96E-4	1.93
	160	1.03E-5	2.11	5.26E-5	2.29	1.00E-5	2.03	5.03E-5	1.97
	320	2.56E-6	2.02	1.30E-5	2.01	2.49E-6	2.02	1.27E-5	1.98
P^2	10	1.68E-4		8.22E-4		1.30E-4		7.86E-4	
	20	1.77E-5	3.25	1.03E-4	2.99	1.60E-5	3.01	1.02E-4	2.94
	40	2.09E-6	3.07	1.28E-5	3.01	1.99E-6	3.00	1.28E-5	2.99
	80	2.62E-7	3.00	2.03E-6	2.65	2.49E-7	3.00	1.61E-6	3.00
	160	3.11E-8	3.07	2.01E-7	3.33	3.11E-8	3.00	2.01E-7	3.00
	320	3.89E-9	3.00	2.52E-8	3.00	3.89E-9	3.00	2.52E-8	3.00
P^3	10	5.14E-5		1.83E-4		5.04E-6		3.64E-5	
	20	2.71E-6	4.24	1.63E-5	3.49	3.11E-7	4.01	2.29E-6	3.99
	40	1.94E-8	7.12	1.44E-7	6.82	1.94E-8	4.00	1.44E-7	3.99
	80	1.21E-9	4.00	9.05E-9	4.00	1.21E-9	4.00	9.05E-9	4.00
	160	7.57E-11	4.00	5.66E-10	4.00	7.57E-11	4.00	5.66E-10	4.00
	320	4.73E-12	4.00	3.53E-11	4.00	4.73E-12	4.00	3.54E-11	4.00

$t)$). We compute the solution up to $t=2$. The errors and numerical orders of accuracy of the density for the RKDG method with the HWENO limiter comparing with the original RKDG method without a limiter are shown in Table 2. Similar to the previous example, we can see that the HWENO limiter keeps the designed order of accuracy.

Example 5.3. We solve the following scalar Burgers equation in two dimensions:

$$\mu_t+\left(\frac{\mu^2}{2}\right)_x+\left(\frac{\mu^2}{2}\right)_y=0, \quad (x,y)\in[0,4]\times[0,4], \tag{5.2}$$

with the initial condition $\mu(x,y,0)=0.5+\sin(\pi(x+y)/2)$ and periodic boundary conditions in both directions. We compute the solution up to $t=0.5/\pi$, when the solution is still smooth. The errors and numerical orders of accuracy for the RKDG method with the HWENO limiter comparing with the original RKDG method without limiter are shown in Table 3. We again observe good results as in the one-dimensional case.

Example 5.4. We solve the Euler equations (4.4). The initial conditions are: $\rho(x,y,0)=1+0.2\sin(\pi(x+y))$, $\mu(x,y,0)=0.7$, $\nu(x,y,0)=0.3$, $p(x,y,0)=1$. The computational domain

Table 3: $\mu_t+\left(\frac{\mu^2}{2}\right)_x+\left(\frac{\mu^2}{2}\right)_y=0$. $\mu(x,y,0)=0.5+\sin(\pi(x+y)/2)$. Periodic boundary condition. $t=0.5/\pi$. L^1 and L^∞ errors. RKDG with the HWENO limiter compared to RKDG without limiter.

		DG with HWENO limiter				DG without limiter			
	cells	L^1 error	order	L^∞ error	order	L^1 error	order	L^∞ error	order
P^1	10×10	3.99E-2		3.27E-1		3.19E-2		3.40E-1	
	20×20	9.78E-3	2.03	1.20E-1	1.44	7.88E-3	2.02	1.05E-1	1.68
	40×40	2.31E-3	2.08	3.28E-2	1.87	1.98E-3	1.99	3.26E-2	1.69
	80×80	5.34E-4	2.11	9.10E-3	1.85	4.92E-4	2.01	9.16E-3	1.83
	160×160	1.23E-4	2.12	2.38E-3	1.93	1.23E-4	2.00	2.40E-3	1.93
P^2	10×10	5.04E-3		1.77E-1		5.20E-3		1.81E-1	
	20×20	8.16E-4	2.62	4.13E-2	2.09	8.29E-4	2.64	4.15E-2	2.12
	40×40	1.12E-4	2.86	6.08E-3	2.77	1.12E-4	2.88	6.03E-3	2.78
	80×80	1.44E-5	2.96	1.00E-3	2.60	1.44E-5	2.96	1.00E-3	2.59
	160×160	1.82E-6	2.98	1.37E-4	2.86	1.82E-6	2.98	1.37E-4	2.86
P^3	10×10	1.91E-3		8.22E-2		1.91E-3		8.29E-2	
	20×20	1.25E-4	3.93	9.16E-3	3.16	1.29E-4	3.89	9.21E-3	3.17
	40×40	8.97E-6	3.80	7.57E-4	3.60	9.11E-6	3.82	7.51E-4	3.61
	80×80	5.80E-7	3.95	5.93E-5	3.67	5.76E-7	3.98	6.03E-5	3.64
	160×160	3.65E-8	3.99	3.97E-6	3.90	3.65E-8	3.98	3.97E-6	3.92

is $(x,y)\in[0,2]\times[0,2]$. Periodic boundary conditions are applied in both directions. The exact solution is $\rho(x,y,t)=1+0.2\sin(\pi(x+y-t))$. We compute the solution up to $t=2$. The errors and numerical orders of accuracy of the density for the RKDG method with the HWENO limiter comparing with the original RKDG method without a limiter are shown in Table 4. The proposed HWENO limiter again keeps the designed order of accuracy.

We now test the performance of the RKDG method with the HWENO limiters for problems containing shocks. From now on, we reset the constant to $C_k=1$. For comparison with the RKDG method using the *minmod* TVB limiter, we refer to the results in [4,7]. For comparison with the RKDG method using the previous versions of HWENO type limiters, we refer to the results in [18,30].

Example 5.5. We consider the 1D Euler equations (3.7) with a Riemann initial condition for the Lax problem: $(\rho,\mu,p)^T=(0.445,0.698,3.528)^T$ for $x\in[-5,0)$; $(\rho,\mu,p)^T=(0.5,0,0.571)^T$ for $x\in[0,5]$. The computed density ρ is plotted at $t=1.3$ against the exact solution in Fig. 1 and the time history of the troubled cells is shown in Fig. 2.

Example 5.6. A higher order scheme would show its advantage when the solution contains both shocks and complex smooth region structures. A typical example for this is the problem of shock interaction with entropy waves [26]. We solve the Euler equations (3.7) with a moving Mach= 3 shock interacting with sine waves in density: $(\rho,\mu,p)^T=$

Table 4: 2D-Euler equations: initial data $\rho(x,y,0)=1+0.2\sin(\pi(x+y))$, $\mu(x,y,0)=0.7$, $\nu(x,y,0)=0.3$, and $p(x,y,0)=1$. Periodic boundary condition. $t=2.0$. L^1 and L^∞ errors. RKDG with the HWENO limiter compared to RKDG without limiter.

		DG with HWENO limiter				DG without limiter			
	cells	L^1 error	order	L^∞ error	order	L^1 error	order	L^∞ error	order
P^1	10×10	4.16E-2		7.98E-2		2.55E-2		4.44E-2	
	20×20	5.61E-3	2.89	1.81E-2	2.13	3.72E-3	2.78	7.71E-3	2.52
	40×40	7.83E-4	2.84	3.80E-3	2.25	5.29E-4	2.81	1.51E-3	2.35
	80×80	1.17E-4	2.73	7.02E-4	2.44	9.14E-5	2.53	4.73E-4	1.67
	160×160	2.49E-5	2.24	1.63E-4	2.10	1.89E-5	2.27	1.30E-4	1.86
P^2	10×10	7.94E-4		5.71E-3		7.95E-4		5.52E-3	
	20×20	1.06E-4	2.90	9.23E-4	2.63	1.02E-4	2.95	8.78E-4	2.65
	40×40	1.34E-5	2.98	1.43E-4	2.69	1.25E-5	3.03	1.28E-4	2.77
	80×80	1.48E-6	3.17	1.70E-5	3.07	1.49E-6	3.07	1.70E-5	2.91
	160×160	1.81E-7	3.04	2.17E-6	2.97	1.81E-7	3.04	2.17E-6	2.97
P^3	10×10	4.10E-4		9.86E-4		4.86E-5		6.70E-4	
	20×20	2.85E-6	7.16	4.04E-5	4.60	2.85E-6	4.08	4.04E-5	4.05
	40×40	1.75E-7	4.02	2.49E-6	4.02	1.75E-7	4.03	2.49E-6	4.02
	80×80	1.08E-8	4.01	1.55E-7	4.01	1.08E-8	4.02	1.55E-7	4.01
	160×160	6.76E-10	4.00	9.71E-9	4.00	6.76E-10	4.00	9.71E-9	4.00

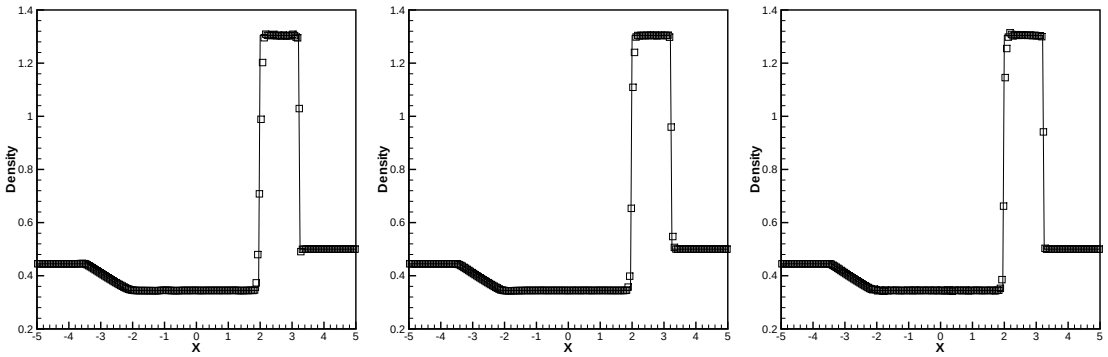

Figure 1: The Lax problem. RKDG with the HWENO limiter. Solid line: the exact solution; squares: numerical solution. Left: second order (P^1); middle: third order (P^2); right: fourth order (P^3). Cells: 200.

$(3.857143,2.629369,10.333333)^T$ for $x\in[-5,-4)$; $(\rho,\mu,p)^T=(1+0.2\sin(5x),0,1)^T$ for $x\in[-4,5]$. The computed density ρ is plotted at $t=1.8$ against the referenced "exact" solution which is a converged solution computed by the fifth order finite difference WENO scheme [13] with 2000 grid points in Fig. 3 and the time history of the troubled cells is shown in Fig. 4.

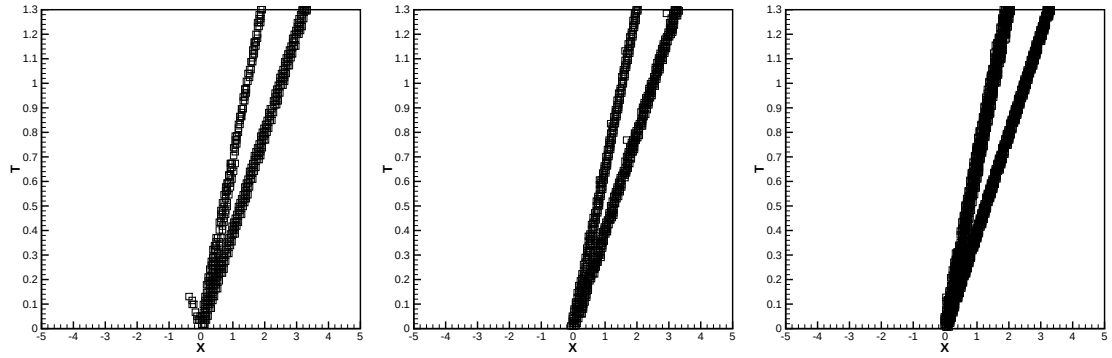

Figure 2: The Lax problem. RKDG with the HWENO limiter. Troubled cells. Squares denote cells which are identified as troubled cells subject to the HWENO limiting. Left: second order (P^1); middle: third order (P^2); right: fourth order (P^3). Cells: 200.

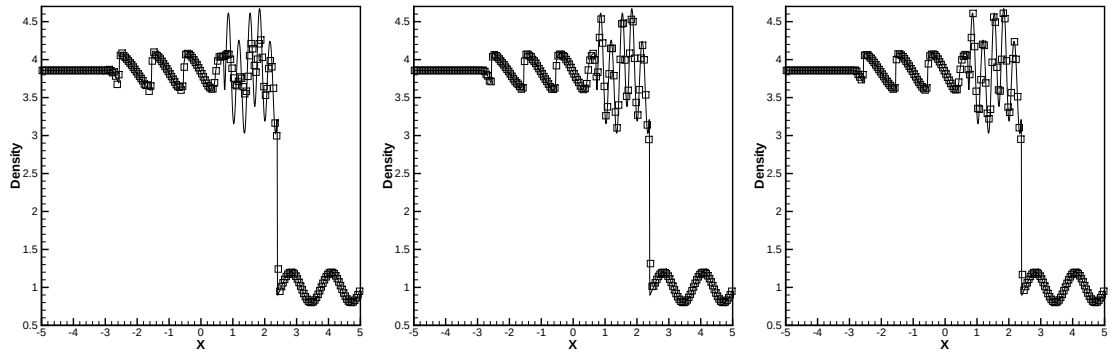

Figure 3: The shock density wave interaction problem. RKDG with the HWENO limiter. Solid line: the "exact" solution; squares: numerical solution. Left: second order (P^1); middle: third order (P^2); right: fourth order (P^3). Cells: 200.

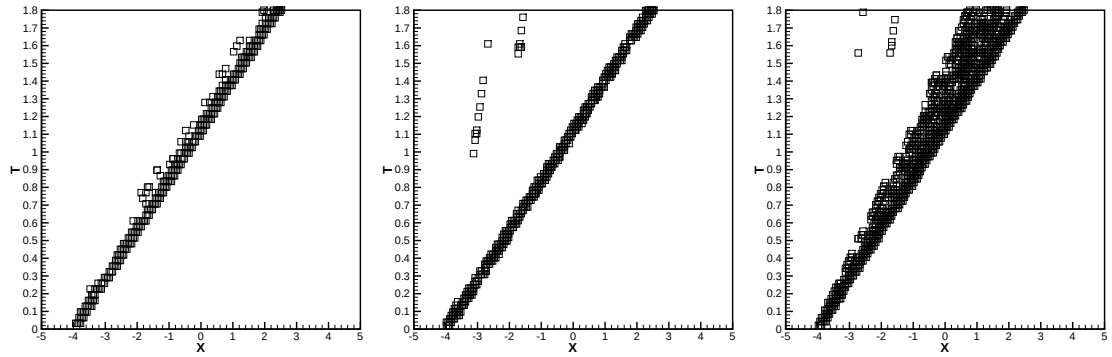

Figure 4: The shock density wave interaction problem. RKDG with the HWENO limiter. Troubled cells. Squares denote cells which are identified as troubled cells subject to the HWENO limiting. Left: second order (P^1); middle: third order (P^2); right: fourth order (P^3). Cells: 200.

Example 5.7. We consider the interaction of blast waves of Euler equation (3.7) with the initial conditions: $(\rho,\mu,p)^T=(1,0,1000)^T$ for $x\in[0,0.1)$; $(\rho,\mu,p)^T=(1,0,0.01)^T$ for $x\in[0.1,0.9)$; $(\rho,\mu,p)^T=(1,0,100)^T$ for $x\in[0.9,1.0]$. The computed density ρ is plotted at $t=0.038$ against the reference "exact" solution which is a converged solution computed by the fifth order finite difference WENO scheme [13] with 2000 grid points in Fig. 5 and the time history of the troubled cells is shown in Fig. 6. We observe that the new RKDG methods do a better job than that in [29].

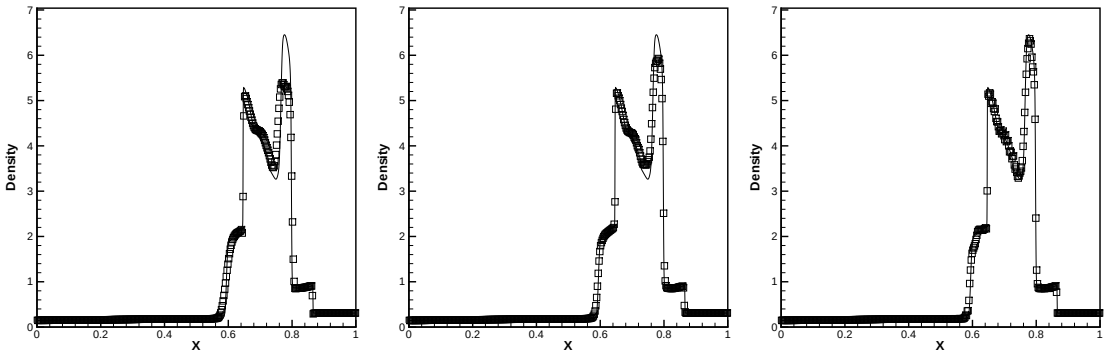

Figure 5: The blast wave problem. RKDG with the HWENO limiter. Solid line: the "exact" solution; squares: numerical solution. Left: second order (P^1); middle: third order (P^2); right: fourth order (P^3). Cells: 400.

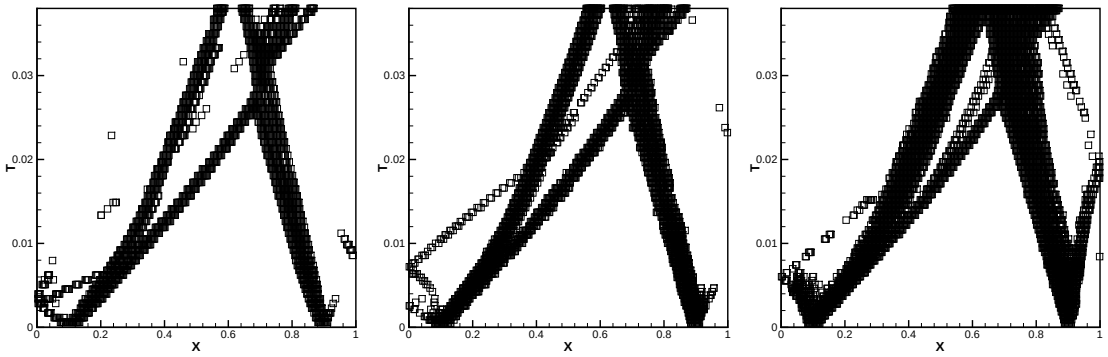

Figure 6: The blast wave problem. RKDG with the HWENO limiter. Troubled cells. Squares denote cells which are identified as troubled cells subject to the HWENO limiting. Left: second order (P^1); middle: third order (P^2); right: fourth order (P^3). Cells: 400.

Remark 5.1. For the P^3 case, the RKDG methods with the WENO limiters specified in [29] used the positivity-preserving limiter to avoid negative density or negative pressure during the time evolution, but the resolution was affected, especially for the smearing of contact discontinuities. The RKDG methods with the new HWENO limiters in this paper can work well without the help from the positivity-preserving limiter.

Example 5.8. The Sedov blast wave problem. This problem contains very low density with strong shocks. The exact solution is specified in detail in [14,23]. The computational domain is $[-2,2]$ and initial conditions are: $\rho=1$, $\mu=0$ and $E=10^{-12}$ everywhere except that the energy in the center cell is the constant $\frac{3200000}{\Delta x}$ (emulating a δ-function at the center). The final computational time is $t=0.001$. The computational results including the density, velocity and pressure pictures are shown in Figs. 7 to 9. The time history of the troubled cells is shown in Fig. 10. The RKDG methods with the original WENO limiters in [29] would break down for this problem without the help of positivity-preserving limiters, yet the new limiter in this paper works well.

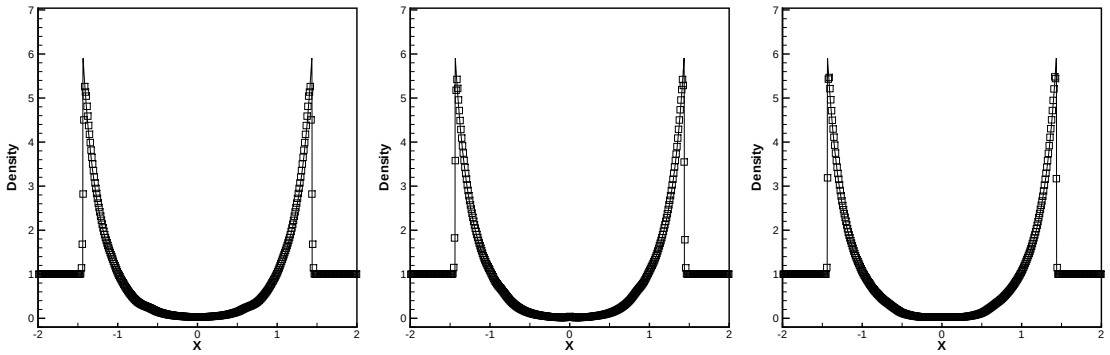

Figure 7: The Sedov blast wave problem. RKDG with the HWENO limiter. Density. Solid line: the exact solution; squares: numerical solution. Left: second order (P^1); middle: third order (P^2); right: fourth order (P^3). Cells: 400.

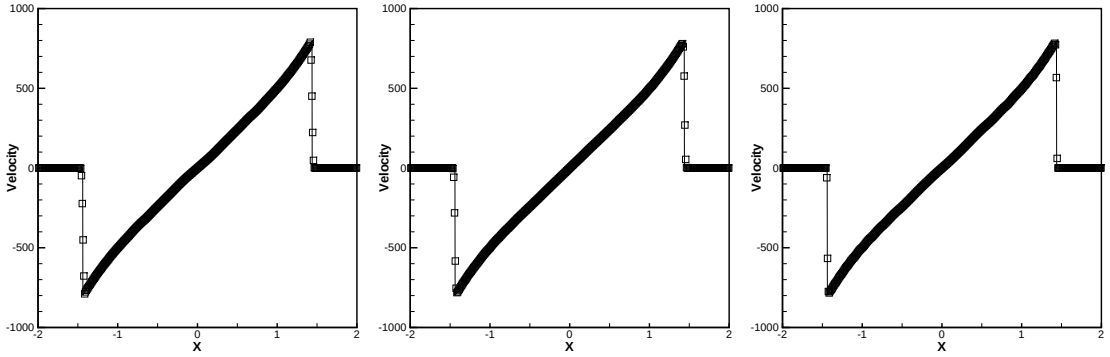

Figure 8: The Sedov blast wave problem. RKDG with the HWENO limiter. Velocity. Solid line: the exact solution; squares: numerical solution. Left: second order (P^1); middle: third order (P^2); right: fourth order (P^3). Cells: 400.

Example 5.9. The double rarefaction wave problem [16]. This test case has low pressure and low density regions and is difficult to simulate. The initial conditions are: $(\rho,\mu,p)^T=$

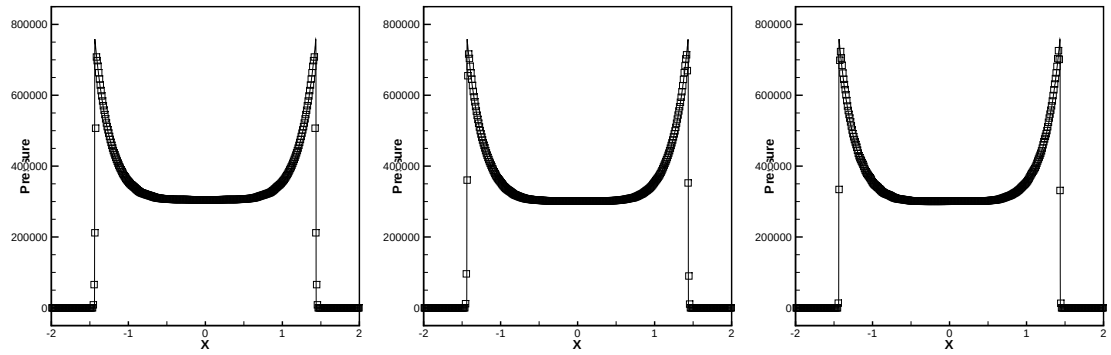

Figure 9: The Sedov blast wave problem. RKDG with the HWENO limiter. Pressure. Solid line: the exact solution; squares: numerical solution. Left: second order (P^1); middle: third order (P^2); right: fourth order (P^3). Cells: 400.

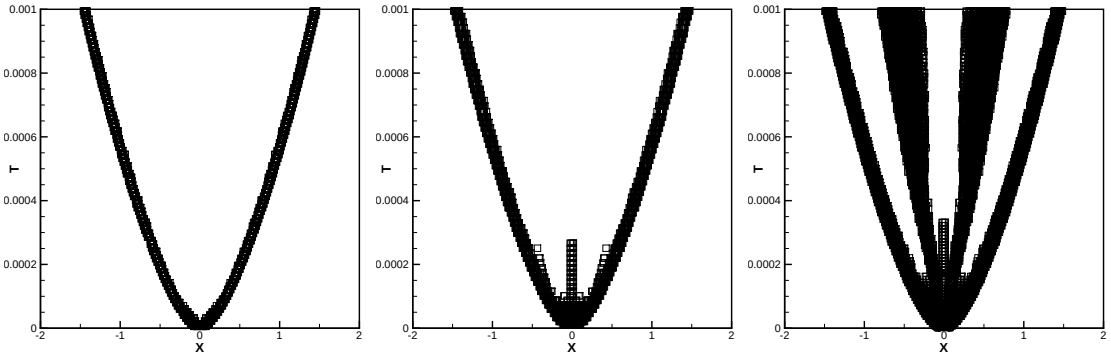

Figure 10: The Sedov blast wave problem. RKDG with the HWENO limiter. Troubled cells. Squares denote cells which are identified as troubled cells subject to the HWENO limiting. Left: second order (P^1); middle: third order (P^2); right: fourth order (P^3). Cells: 400.

$(7,-1,0.2)^T$ for $x\in[-1,0)$; $(\rho,\mu,p)^T=(7,1,0.2)^T$ for $x\in[0,1]$. The final computational time is $t=0.6$. The computational results including the density, velocity and pressure pictures are shown in Figs. 11 to 13. The time history of the troubled cells is shown in Fig. 14. For the P^3 case, the RKDG methods with the WENO limiters in [29] do not work for this problem without the help of positivity-preserving limiters, however the same RKDG methods with the new HWENO limiters in this paper produce good results.

Example 5.10. Double Mach reflection problem. This model problem is originally from [28]. We solve the Euler equations (4.4) in a computational domain of $[0,4]\times[0,1]$. The reflection boundary condition is used at the wall, which for the rest of the bottom boundary (the part from $x=0$ to $x=\frac{1}{6}$), the exact post-shock condition is imposed. At the top boundary is the exact motion of the Mach 10 shock. The results shown are at $t=0.2$. Three different orders of accuracy for the RKDG with HWENO limiters, k=1, k=2 and

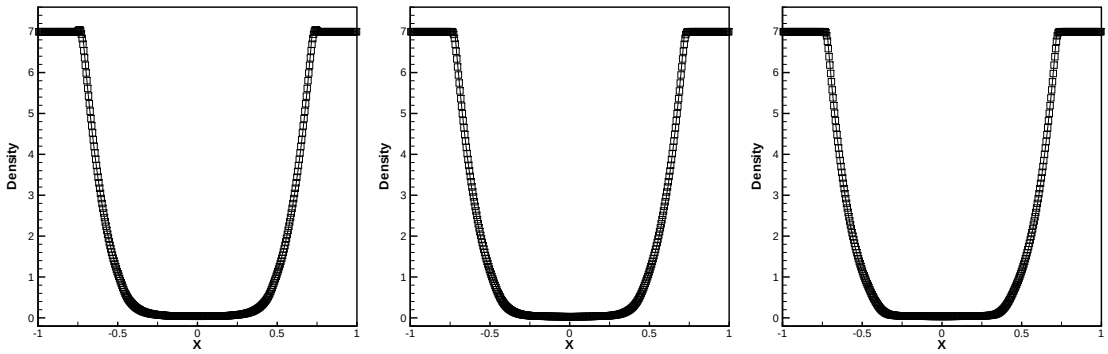

Figure 11: The double rarefaction wave problem. RKDG with the HWENO limiter. Density. Solid line: the exact solution; squares: numerical solution. Left: second order (P^1); middle: third order (P^2); right: fourth order (P^3). Cells: 400.

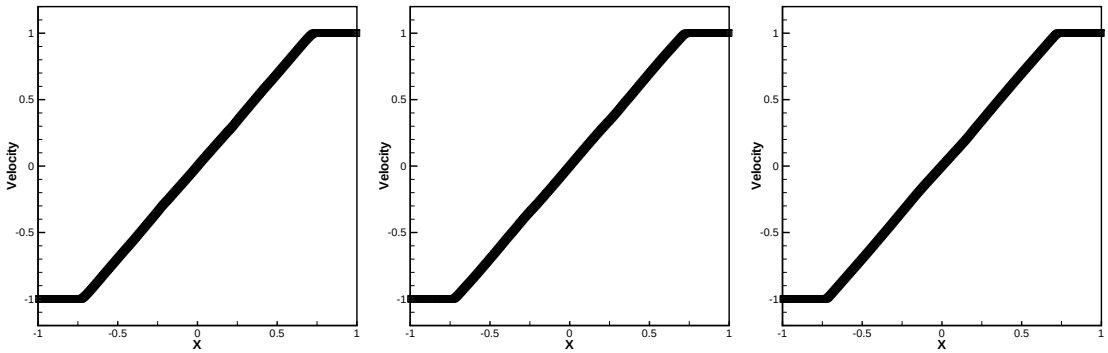

Figure 12: The double rarefaction wave problem. RKDG with the HWENO limiter. Velocity. Solid line: the exact solution; squares: numerical solution. Left: second order (P^1); middle: third order (P^2); right: fourth order (P^3). Cells: 400.

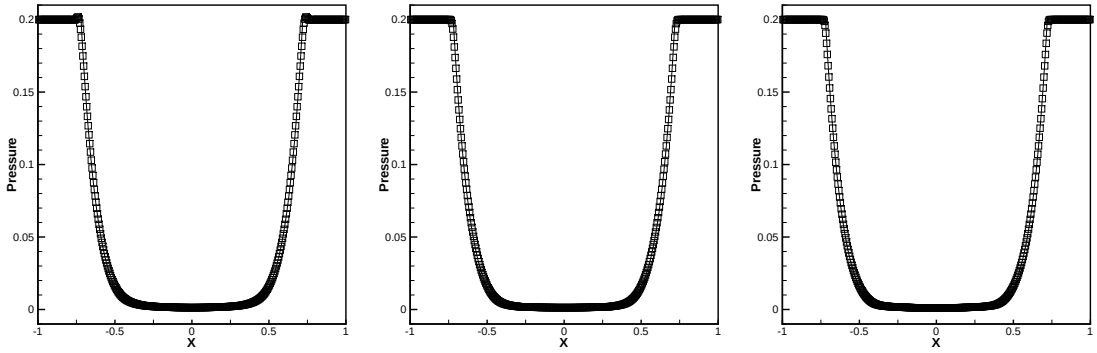

Figure 13: The double rarefaction wave problem. RKDG with the HWENO limiter. Pressure. Solid line: the exact solution; squares: numerical solution. Left: second order (P^1); middle: third order (P^2); right: fourth order (P^3). Cells: 400.

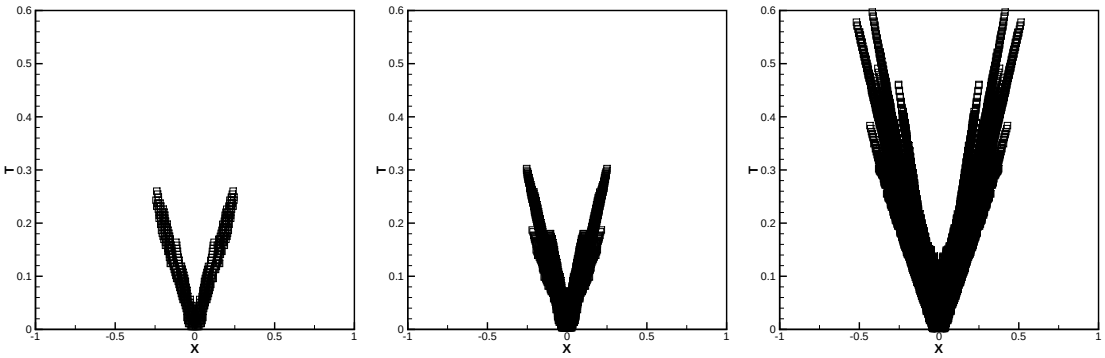

Figure 14: The double rarefaction wave problem. RKDG with the HWENO limiter. Troubled cells. Squares denote cells which are identified as troubled cells subject to the HWENO limiting. Left: second order (P^1); middle: third order (P^2); right: fourth order (P^3). Cells: 400.

k=3 (second order, third order and fourth order), are used in the numerical experiments. The simulation results are shown in Fig. 15. The "zoomed-in" pictures around the double Mach stem to show more details are given in Fig. 16. The troubled cells identified at the

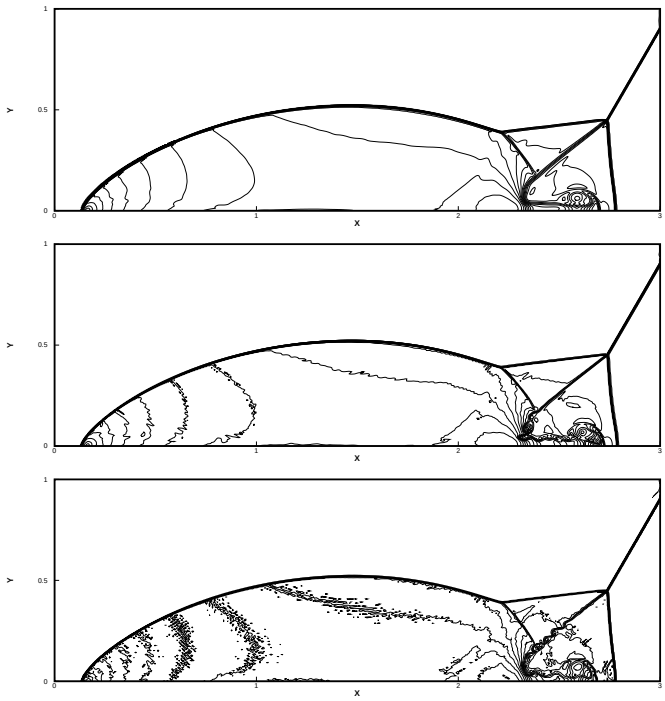

Figure 15: Double Mach refection problem. RKDG with the HWENO limiter. 30 equally spaced density contours from 1.5 to 21.5. Top: second order (P^1); middle: third order (P^2); bottom: fourth order (P^3). Cells: 800 $\times$ 200.

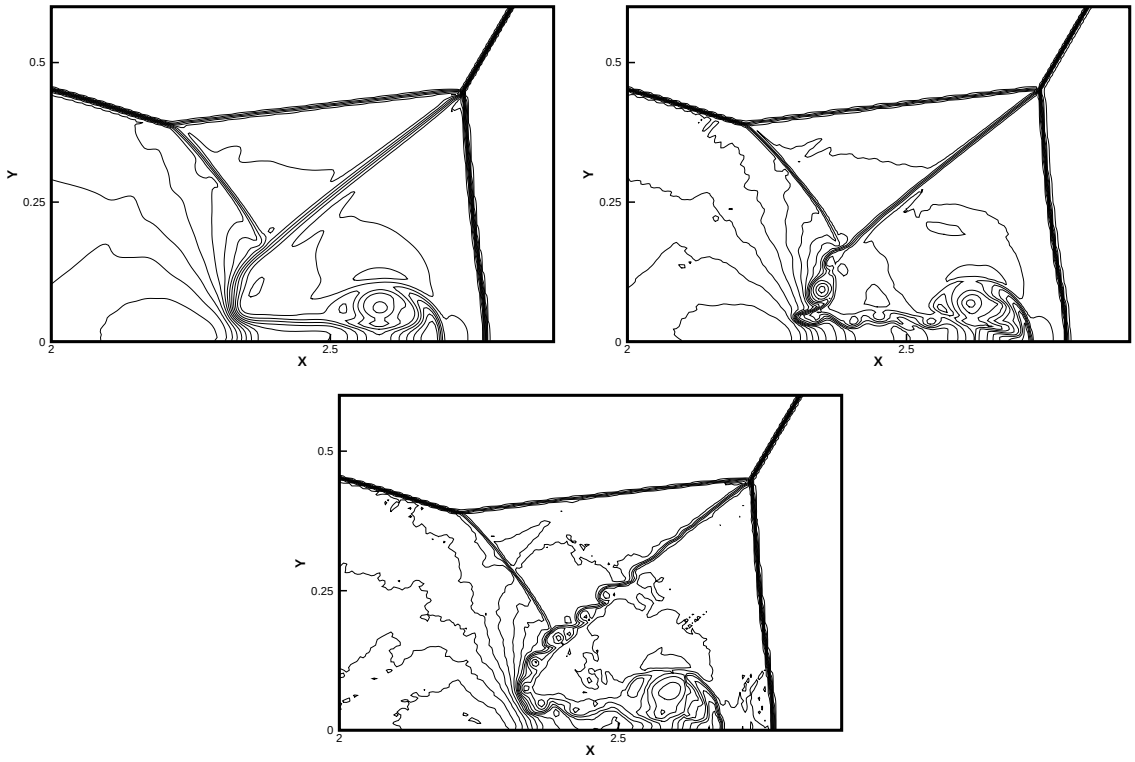

Figure 16: Double Mach refection problem. RKDG with HWENO limiter. Zoom-in pictures around the Mach stem. 30 equally spaced density contours from 1.5 to 21.5. Left: second order (P^1); right: third order (P^2); bottom: fourth order (P^3). Cells: 800 $\times$ 200.

last time step are shown in Fig. 17. Clearly, the resolution improves with an increasing k on the same mesh.

6 Concluding remarks

We have constructed a class of Hermite weighted essentially non-oscillatory (WENO) limiters, based on the procedure of [29], for the Runge-Kutta discontinuous Galerkin (RKDG) methods. The general framework of such HWENO limiters for RKDG methods, namely first identifying troubled cells subject to the HWENO limiting, then reconstructing the polynomial solution inside the troubled cell by the freedoms of the solutions of the DG method on the target cell and its adjacent neighboring cells by a HWENO procedure in a least square sense [8], is followed in this paper. The main novelty of this paper is the HWENO reconstruction procedure, which uses only the information from the troubled cell and its immediate neighbors (two cells in 1D and four cells in 2D), without any other extensive usage of geometric information of the meshes, and with simple positive

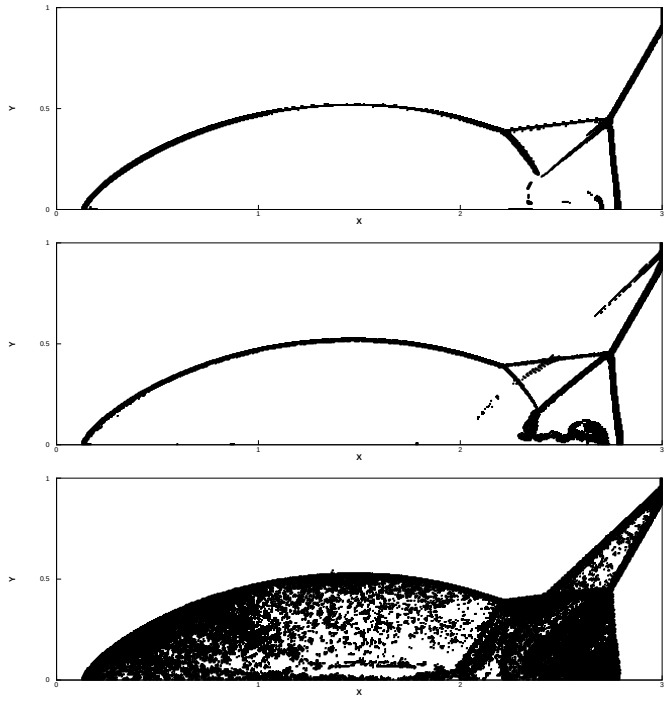

Figure 17: Double Mach refection problem. RKDG with the HWENO limiter. Troubled cells. Squares denote cells which are identified as troubled cells subject to the HWENO limiting. Top: second order (P^1); middle: third order (P^2); bottom: fourth order (P^3). Cells: 800 $\times$ 200.

linear weights in the reconstruction procedure. The methodology in this paper is more sophisticated than the original one specified in [29], but it leads to better resolutions for some examples for the P^3 case, such as those in Example 5.7 to Example 5.10, without the help of positivity-preserving limiters, in one and two dimensions. Numerical results are provided to demonstrate good results, both in accuracy and in non-oscillatory performance, comparable with those in earlier literature with more complicated WENO [20,21] or HWENO [18,19,22] limiters. In the future we will extend this limiter to unstructured meshes and to higher order polynomials (p-version DG methods).

Acknowledgments

The research was partially supported by NSFC grant 11372005, 91230110 and 11328104 and DOE grant DE-FG02-08ER25863 and NSF grant DMS-1418750.

References

[1] D. S. Balsara and C.-W. Shu, *Monotonicity preserving weighted essentially non-oscillatory schemes with increasingly high order of accuracy*, Journal of Computational Physics, 160 (2000), 405-452.

[2] R. Biswas, K.D. Devine and J. Flaherty, *Parallel, adaptive finite element methods for conservation laws*, Applied Numerical Mathematics, 14 (1994), 255-283.
[3] A. Burbeau, P. Sagaut and C.H. Bruneau, *A problem-independent limiter for high-order Runge-Kutta discontinuous Galerkin methods*, Journal of Computational Physics, 169 (2001), 111-150.
[4] B. Cockburn, S. Hou and C.-W. Shu, *The Runge-Kutta local projection discontinuous Galerkin finite element method for conservation laws IV: the multidimensional case*, Mathematics of Computation, 54 (1990), 545-581.
[5] B. Cockburn, S.-Y. Lin and C.-W. Shu, *TVB Runge-Kutta local projection discontinuous Galerkin finite element method for conservation laws III: one dimensional systems*, Journal of Computational Physics, 84 (1989), 90-113.
[6] B. Cockburn and C.-W. Shu, *TVB Runge-Kutta local projection discontinuous Galerkin finite element method for conservation laws II: general framework*, Mathematics of Computation, 52 (1989), 411-435.
[7] B. Cockburn and C.-W. Shu, *The Runge-Kutta discontinuous Galerkin method for conservation laws V: multidimensional systems*, Journal of Computational Physics, 141 (1998), 199-224.
[8] M. Dumbser, D.S. Balsara, E.F. Toro and C.D. Munz, *A unified framework for the construction of one-step finite-volume and discontinuous Galerkin schemes on unstructured meshes*, Journal of Computational Physics, 227 (2008), 8209-8253.
[9] M. Dumbser and M. Käser, *Arbitrary high order non-oscillatory finite volume schemes on unstructured meshes for linear hyperbolic systems*, Journal of Computational Physics, 221 (2007), 693-723.
[10] M. Dumbser, O. Zanotti, R. Loubère and S. Diot, *A posteriori subcell limiting of the discontinuous Galerkin finite element method for hyperbolic conservation laws*, Journal of Computational Physics, 278 (2014), 47-75.
[11] O. Friedrichs, *Weighted essentially non-oscillatory schemes for the interpolation of mean values on unstructured grids*, Journal of Computational Physics, 144 (1998), 194-212.
[12] C. Hu and C.-W. Shu, *Weighted essentially non-oscillatory schemes on triangular meshes*, Journal of Computational Physics, 150 (1999), 97-127.
[13] G. Jiang and C.-W. Shu, *Efficient implementation of weighted ENO schemes*, Journal of Computational Physics, 126 (1996), 202-228.
[14] V.P. Korobeinikov, Problems of Point-Blast Theory, American Institute of Physics, 1991.
[15] L. Krivodonova, J. Xin, J.-F. Remacle, N. Chevaugeon and J.E. Flaherty, *Shock detection and limiting with discontinuous Galerkin methods for hyperbolic conservation laws*, Applied Numerical Mathematics, 48 (2004), 323-338.
[16] T. Linde, P.L. Roe, Robust Euler codes, in: 13th Computational Fluid Dynamics Conference, AIAA Paper-97-2098.
[17] X. Liu, S. Osher and T. Chan, *Weighted essentially non-oscillatory schemes*, Journal of Computational Physics, 115 (1994), 200-212.
[18] H. Luo, J.D. Baum and R. Lohner, *A Hermite WENO-based limiter for discontinuous Galerkin method on unstructured grids*, Journal of Computational Physics, 225 (2007), 686-713.
[19] J. Qiu and C.-W. Shu, *Hermite WENO schemes and their application as limiters for Runge-Kutta discontinuous Galerkin method: one dimensional case*, Journal of Computational Physics, 193 (2003), 115-135.
[20] J. Qiu and C.-W. Shu, *Runge-Kutta discontinuous Galerkin method using WENO limiters*, SIAM Journal on Scientific Computing, 26 (2005), 907-929.
[21] J. Qiu and C.-W. Shu, *A comparison of troubled-cell indicators for Runge-Kutta discontinuous Galerkin methods using weighted essentially nonoscillatory limiters*, SIAM Journal on Scientific

Computing, 27 (2005), 995-1013.
[22] J. Qiu and C.-W. Shu, *Hermite WENO schemes and their application as limiters for Runge-Kutta discontinuous Galerkin method II: two dimensional case*, Computers and Fluids, 34 (2005), 642-663.
[23] L.I. Sedov, Similarity and Dimensional Methods in Mechanics, Academic Press, New York, 1959.
[24] C.-W. Shu, *Essentially non-oscillatory and weighted essentially non-oscillatory schemes for hyperbolic conservation laws*, In Advanced Numerical Approximation of Nonlinear Hyperbolic Equations, B. Cockburn, C. Johnson, C.-W. Shu and E. Tadmor (Editor: A. Quarteroni), Lecture Notes in Mathematics, volume 1697, Springer, 1998, 325-432.
[25] C.-W. Shu and S. Osher, *Efficient implementation of essentially non-oscillatory shock-capturing schemes*, Journal of Computational Physics, 77 (1988), 439-471.
[26] C.-W. Shu and S. Osher, *Efficient implementation of essentially non-oscillatory shock capturing schemes II*, Journal of Computational Physics, 83 (1989), 32-78.
[27] C. Wang, X. Zhang, C.-W. Shu and J. Ning, *Robust high order discontinuous Galerkin schemes for two-dimensional gaseous detonations*, Journal of Computational Physics, 231 (2012), 653-665.
[28] P. Woodward and P. Colella, *The numerical simulation of two-dimensional fluid flow with strong shocks*, Journal of Computational Physics, 54 (1984), 115-173.
[29] X. Zhong and C.-W. Shu, *A simple weighted essentially nonoscillatory limiter for Runge-Kutta discontinuous Galerkin methods*, Journal of Computational Physics, 232 (2013), 397-415.
[30] J. Zhu, J. Qiu, C.-W. Shu and M. Dumbser, *Runge-Kutta discontinuous Galerkin method using WENO limiters II: Unstructured meshes*, Journal of Computational Physics, 227 (2008), 4330-4353.
[31] J. Zhu, X. Zhong, C.-W. Shu and J.X. Qiu, *Runge-Kutta discontinuous Galerkin method using a new type of WENO limiters on unstructured meshes*, Journal of Computational Physics, 248 (2013), 200-220.